



Australia's National
Science Agency

GISERA | Gas Industry Social and Environmental Research Alliance

Establishing Baseline Groundwater and Natural Seismicity Levels across the Northern Perth Basin with Passive Seismic Data – Interim Report 2

Baseline Groundwater and Seismicity of Northern Perth Basin

1 May 2025



Australian Government
Department of Industry,
Science and Resources



Supported by
Government of
South Australia



NORTHERN
TERRITORY
GOVERNMENT



QGC

Santos

tamboran
RESOURCES



Citation

Peng Guo, Mehdi Tork Qashqai and Erdinc Saygin (2025), Establishing Baseline Groundwater and Natural Seismicity Levels across the Northern Perth Basin with Passive Seismic Data – Interim Report 2. CSIRO, Australia.

Copyright

© Commonwealth Scientific and Industrial Research Organisation 2024. To the extent permitted by law, all rights are reserved and no part of this publication covered by copyright may be reproduced or copied in any form or by any means except with the written permission of CSIRO.

Important disclaimer

CSIRO advises that the information contained in this publication comprises general statements based on scientific research. The reader is advised and needs to be aware that such information may be incomplete or unable to be used in any specific situation. No reliance or actions must therefore be made on that information without seeking prior expert professional, scientific and technical advice. To the extent permitted by law, CSIRO (including its employees and consultants) excludes all liability to any person for any consequences, including but not limited to all losses, damages, costs, expenses and any other compensation, arising directly or indirectly from using this publication (in part or in whole) and any information or material contained in it.

CSIRO is committed to providing web accessible content wherever possible. If you are having difficulties with accessing this document please contact [csiro.au/contact](https://www.csiro.au/contact).

Contents

1	Executive Summary	0
2	Introduction	0
3	Groundwater level monitoring using seismic waves.....	1
3.1	Seismic data & processing.....	1
3.2	Groundwater & borehole data.....	5
3.3	Baseline shear-wave velocity models and depth sensitivity kernels	7
3.4	Monitoring groundwater level changes using seismic waves.....	9
4	Seismicity detection, phase picking and phase association	14
4.1	Introduction.....	14
4.2	Earthquake detection and phase picking	14
4.3	Phase association and initial earthquake location estimation.....	16
5	Estimation of Earthquake Hypocentres.....	18
5.1	The absolute earthquake locations	18
5.2	The relative location of earthquakes or precise location.....	19

Acknowledgement

This research has been funded through CSIRO's Gas Industry Social and Environmental Research Alliance (GISERA) with contributions from the Australian Government's Department of Industry, Science, Energy and Resources. GISERA is a collaboration between CSIRO, Commonwealth, state and territory governments and industry established to undertake research on the impacts of onshore gas exploration and development on the environment, and the socio-economic costs and benefits. This research uses seismic data (2022-2023) recorded by WA-Array, deployed by Geological Survey of Western Australia. For information about GISERA's governance structure, projects and research findings visit <https://gisera.csiro.au>.

1 Executive Summary

The objective of this report is to provide progress for subsurface velocity changes caused by groundwater level variations and natural seismicity event detection and localising in the Northern Perth Basin. We use seismic data recorded by the WA-Array seismic array in 2022-2023, recently deployed by the Geological Survey of Western Australia (GSWA).

We processed the seismic data from December 2022 to December 2023 to extract Rayleigh wavefields and their coda. Analysis of the seismic waveform changes throughout the one-year data suggests that the seismic velocity of shear waves in the Northern Perth Basin decreases during winter (raining season) and increases at summer (dry season), with the trend inversely correlated to the groundwater depth (hydraulic head) from borehole measurements. Data from the outback (inland) did not show such patterns. Furthermore, we revealed that the time-lapse seismic velocity changes become more pronounced with increasing seismic frequencies, i.e., at the shallower depths (the upper ~400 m). We investigated the feasibility of providing high-resolution spatial maps for velocity changes, but sparse seismometer coverage (~40 km spacing is too large for local-scale study) limited spatial resolution.

To investigate seismicity in the Northern Perth Basin and its surrounding areas, we applied a machine learning-based approach for both earthquake detection and phase picking. The analysis was conducted using seismic data recorded between December 2022 and September 2024. Earthquake locations were determined through an iterative process using multiple methods to progressively refine hypocentre estimates. This approach enabled the identification of numerous earthquakes, including several distinct clusters of seismic activity.

The project is on time for objectives and budget.

2 Introduction

The Northern Perth Basin extends approximately 450 km from north to south and spans up to 90 km from west to east. Covering an area of around 35,000 km², this region constitutes about three-quarters of the onshore portion of the Perth Basin (Department of Water, 2017). It is a geologically significant area that supports diverse resource exploration and extraction activities, for example natural gas production, which plays a crucial role in the region's energy supply.

Monitoring groundwater dynamics is critical for sustainable water resource management, particularly in regions facing increasing water stress due to climate change and anthropogenic pressures. In the Northern Perth Basin, the extraction of natural gas, especially through advanced techniques such as hydraulic fracturing, could place considerable stress on local water supplies. Groundwater level monitoring conducted by the department uses groundwater wells, which provides high-precision point data for groundwater levels (hydraulic heads) but are limited in

spatial coverage and often costly to maintain. Drilling a borehole can also be invasive and expensive. Additionally, Parker et al. (2017) used Interferometric Synthetic Aperture Radar (InSAR) data and mapped ground subsidence of up to 15 mm per year due to groundwater extraction between 2015 and 2016 in the Perth Basin. Yet, InSAR-based measurements only measure changes on the surface and have limited information for the physical mechanisms beneath the surface.

Laboratory and field-scale experiments have shown that seismic S-wave velocities tend to increase with decreasing water content, offering a proxy for estimating water table depth and changes in saturation (e.g., Knight & Endres, 2005; Doussan et al., 1999). Active seismic methods, including reflection and refraction surveys as well as surface wave analysis, have demonstrated sensitivity to changes in subsurface elastic properties caused by variations in water saturation (Park et al., 2007). Passive seismic techniques (Clements & Denolle, 2018; Mao et al., 2022) have gained traction in recent years due to their ability to provide continuous and environmentally friendly monitoring over broad areas.

Moreover, production activities could have the potential to induce small-magnitude earthquake events. Therefore, it is important to establish a baseline catalogue of natural seismicity in the region prior to the commencement of any such activities. This ensures that future industrial operations are not mistakenly perceived as causing excessive seismic activity. Once this baseline is established, statistical analysis can be conducted to estimate the recurrence rates of future earthquakes.

The objective of this project is to measure the seasonal and spatial fluctuations of the hydraulic head of water in aquifers and background seismic activity in the Northern Perth Basin using the statewide passive seismic data currently being acquired by GSWA. Interim report 1 can be found in Guo et al. (2024), where we provided preliminary velocity analysis and seismicity detection. In this report we measured seasonal changes in the seismic wave velocities and their relationship with groundwater levels, along with the associated spatial distributions (Section 3). We also analysed the seismicity (Section 4) and earthquake locations (Section 5).

3 Groundwater level monitoring using seismic waves

3.1 Seismic data & processing

We used the continuous seismic data recorded by the seismic network WA-Array, which was installed and operated by Geological Survey of Western Australia. The phase-1 data was available from November 2022 to December 2023. The survey contains 129 broadband seismic stations. Figure 3.1 shows the location of the seismometers. In this study, our main interest is in the Northern Perth Basin, with the dashed red line indicating the boundary of the Perth Basin. There

are a total of 17 seismometers located within the Perth Basin and the number of seismometers drops to 9 in the Northern Perth Basin. We also included some stations along the boundary of the Perth Basin and all the stations used for time-lapse study were located in the left black rectangle in Figure 3.1. The broad-band seismic stations in the right black rectangle in Figure 3.1 were far away from the Perth Basin and were used as a control group for comparing results. Figure 3.2 shows the recording time duration for each of the seismic stations that is of interest. The seismic stations highlighted with red colours were those located in the Northern Perth Basin.

For the data processing, we detrended and down-sampled the vertical component of the continuously recorded seismic data (most of them are ambient noise) from 100 Hz to 20 Hz with anti-aliasing filtering. The ambient noise data were then filtered to the frequency band 0.05 – 2.5 Hz. 1-bit normalisation was applied to the data in the time domain (Bensen et al., 2007). We divided the recordings of ambient noise into daily-long segments. The daily Green's function (seismic waves travelling between arbitrary two seismic stations/nodes) were then reconstructed by computing cross correlations for all the pairs of stations within 100 km distance using the segmented noise data. The maximum time lag for cross correlation was 120 s. We tested different stacking methods, including linear stacking, robust stacking, phase-weighted stacking and selective stacking (Yuan et al., 2021). The method of robust stacking was chosen for stacking cross-correlation functions within the daily segments. We further stacked over 14 days of the daily cross correlation functions to improve the signal to noise ratio, with a 7-day step. The stacked fortnight data was the monitoring data. To obtain the reference/baseline data for each of the station pair, we stacked all the available fortnight data. We limit the maximum distance of station pairs to be 100 km.

Figure 3.3 shows the obtained cross correlation functions used as reference data from ambient noise interferometry. The dashed red line is the travel time moveout for a velocity of 2 km/s. The data is in general of good quality. Figure 3.4 shows the extracted time-lapse fortnight cross-correlation functions for one station pair, from which we will measure the waveform changes and infer corresponding velocity changes of seismic waves (in this case, the Rayleigh waves), with details given in Section 3.4.

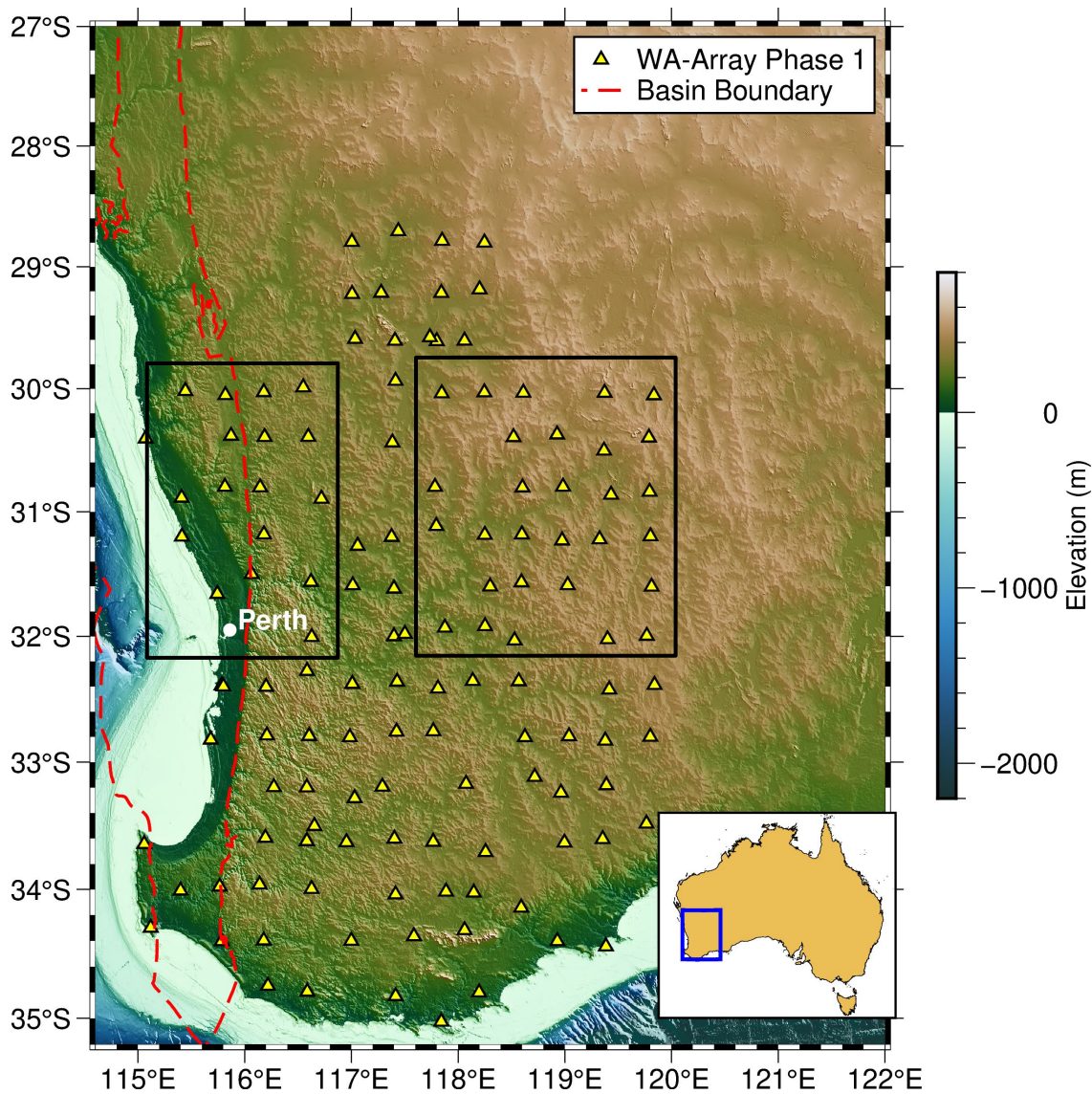


Figure 3.1. Map of the study area. The yellow triangles show the broad-band seismic stations from the Phase 1 of WA-Array. The red dashed line refers to the boundary of the Perth Basin. The black rectangle in the left shows the area of interest for this study, mainly the Northern Perth Basin and the surrounding area. The black rectangle in the right shows the area that is outside the Northern Perth Basin and is used as control group to compare results.

Seismic Station Recording Durations

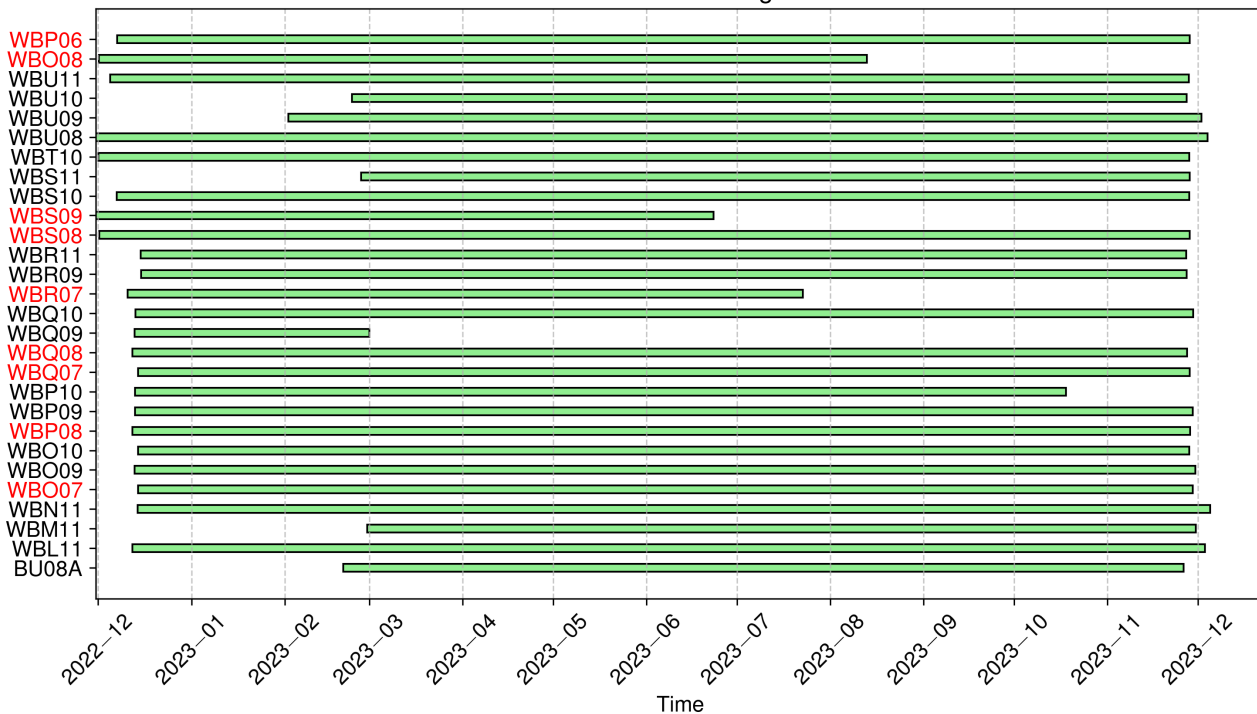


Figure 3.2. The recording time duration for seismic stations used in this study. The labels on the Y axis are the names for the broad-band seismic stations located within the left black rectangle in Figure 3.1. Seismic stations that are located in the Northern Perth Basin (left of the red dashed line in Figure 3.1) are highlighted using the red color. The labels on the X axis are in the format of “Year-Month”.

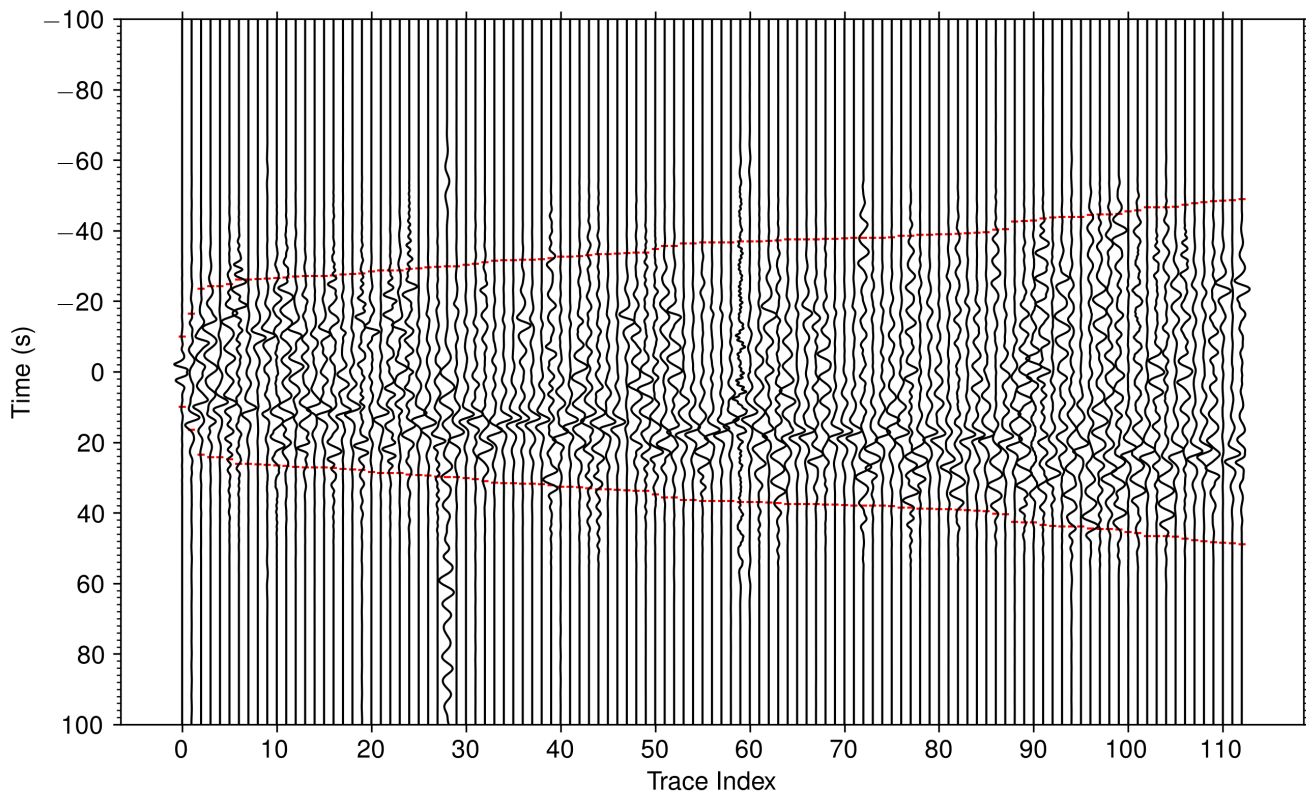


Figure 3.3. Cross-correlation functions for all the stations pairs in the area of interest (the left black rectangle in Figure 3.1). The station pairs were sorted with station-pair distance, with the maximum distance being 100 km as we are studying local velocity changes. The Y axis is temporal lags for cross correlation. The dashed red line marks the move out with a velocity of 2 km/s.

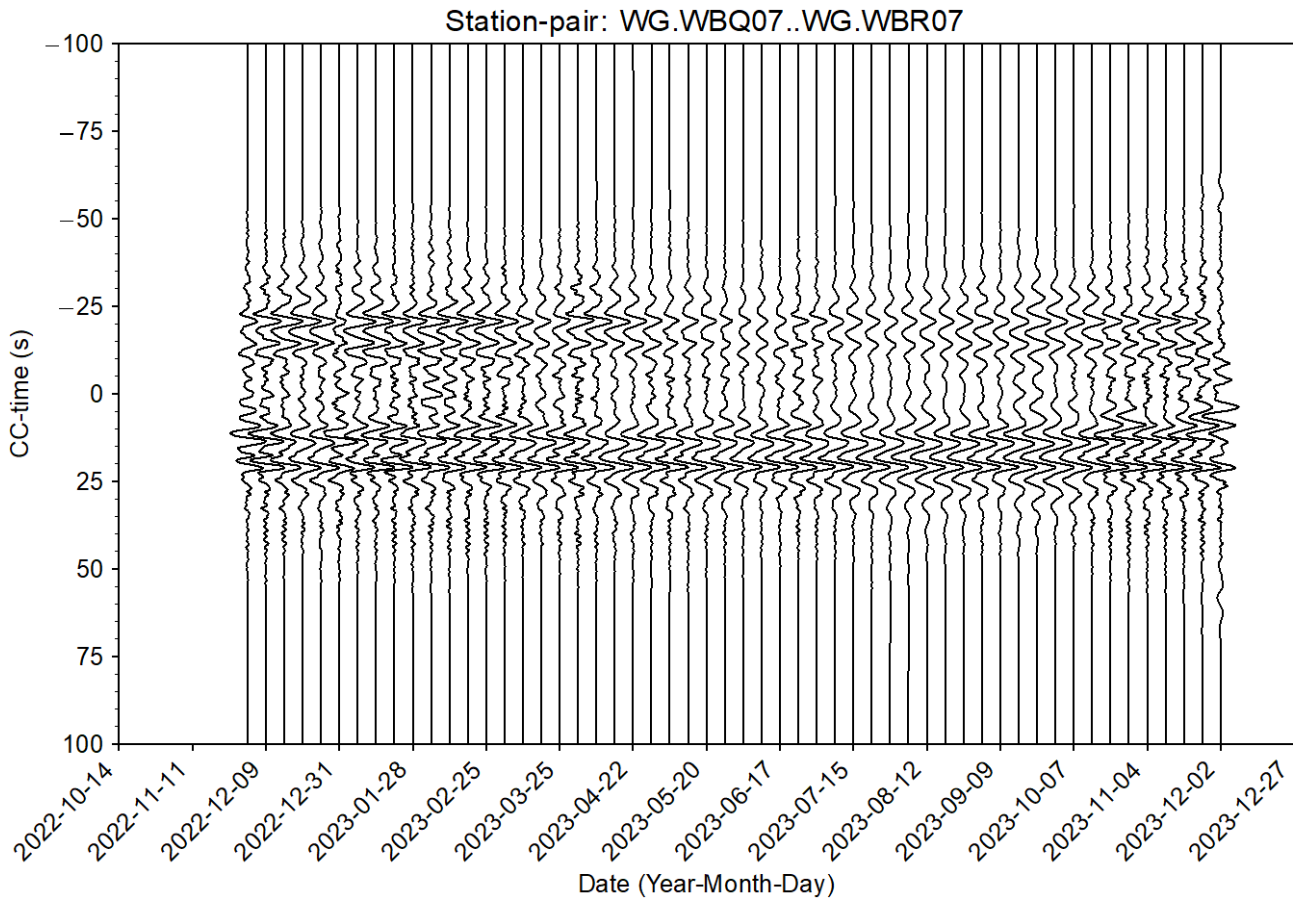


Figure 3.4. Time-lapse cross-correlation functions on a fortnight interval for the station pair WBQ07 and WBR07 (station names were given in Figure 3.5b). The Y axis is temporal lags for cross correlation.

3.2 Groundwater & borehole data

Figure 3.5a shows the distribution of all the borehole groundwater wells in WA (source: <https://wir.water.wa.gov.au/Pages/Water-Information-Reporting.aspx>). However, most of these wells were read annually (personal communication with Philip Commander, formerly Principal Hydrogeologist at the Department of Water and Environmental Regulation, WA) and many have been abandoned. When filtered the database using keyword “monitoring” and choosing “telemetered data only”, it narrowed down to 76 wells (Figure 3.5b). The telemetered sites were

limited to the Perth metropolitan region where groundwater is intensively used, with monthly data readings.

We downloaded the borehole groundwater monitoring data from Water Information Reporting, Department of Water and Environmental Regulation (<https://wir.water.wa.gov.au/Pages/Water-Information-Reporting.aspx>). Figure 3.6a shows the groundwater level (hydraulic head) from December 2022 to December 2023 from the telemetered wells, with each line corresponding to a borehole. Figure 3.6b shows the temporal data variations for each borehole, by subtract the groundwater level from its mean. Figure 3.6c is the same data with Figure 3.6b, but we limit the range of groundwater level variation to be -1 and 1 m. We noticed that for the Perth metropolitan region, even it was a relatively small area compared to the seismic station spacing, the difference in the groundwater level were significant, from ~-20 m to ~70 m. For the temporal changes of the groundwater levels, majority of the variations were within 1 m in 2022-2023.

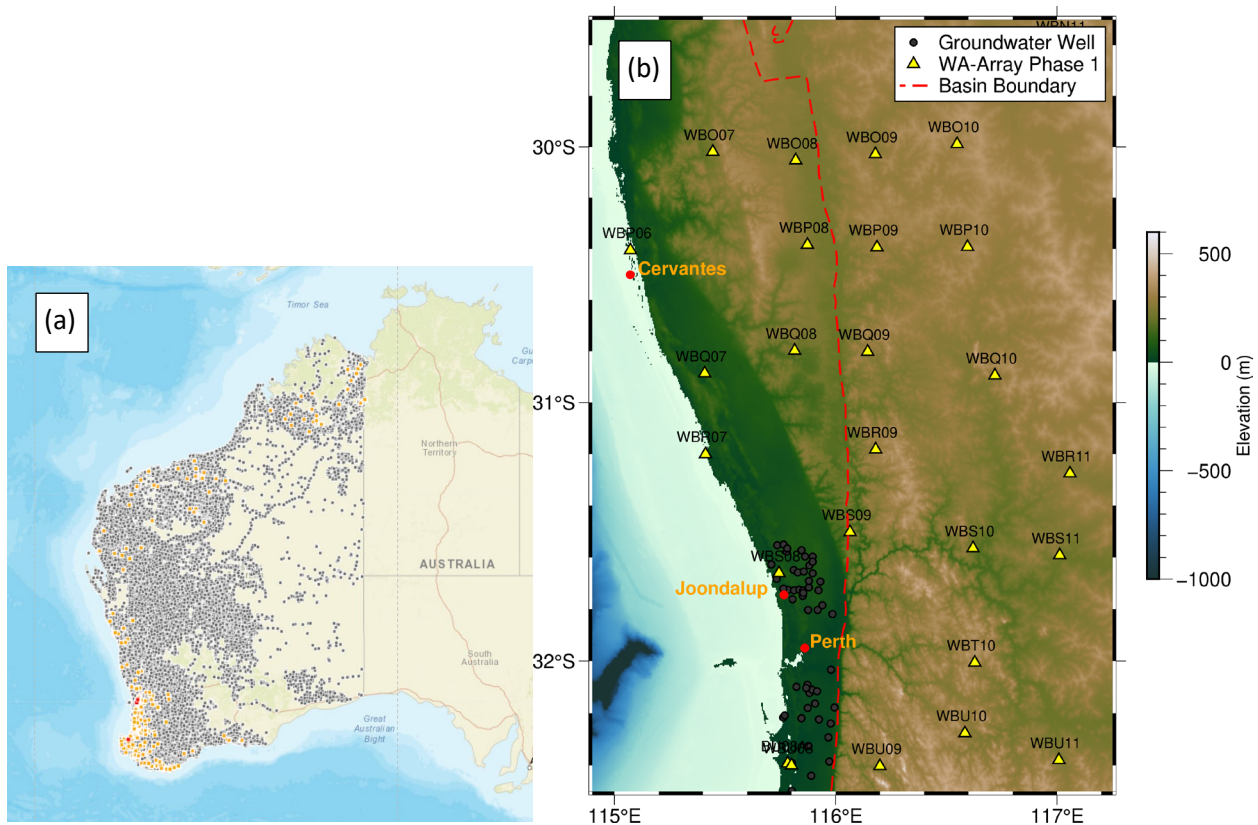


Figure 3.5 The location of borehole groundwater wells. (a) shows all the boreholes in Western Australia (data from <https://wir.water.wa.gov.au/Pages/Water-Information-Reporting.aspx>). (b) shows the telemetered groundwater boreholes (black circles, monthly readings) and seismic stations (yellow triangles) for this study. The dashed red line refers to the boundary of the Perth Basin. We also labelled the location of Perth city, Joondalup and Cervantes.

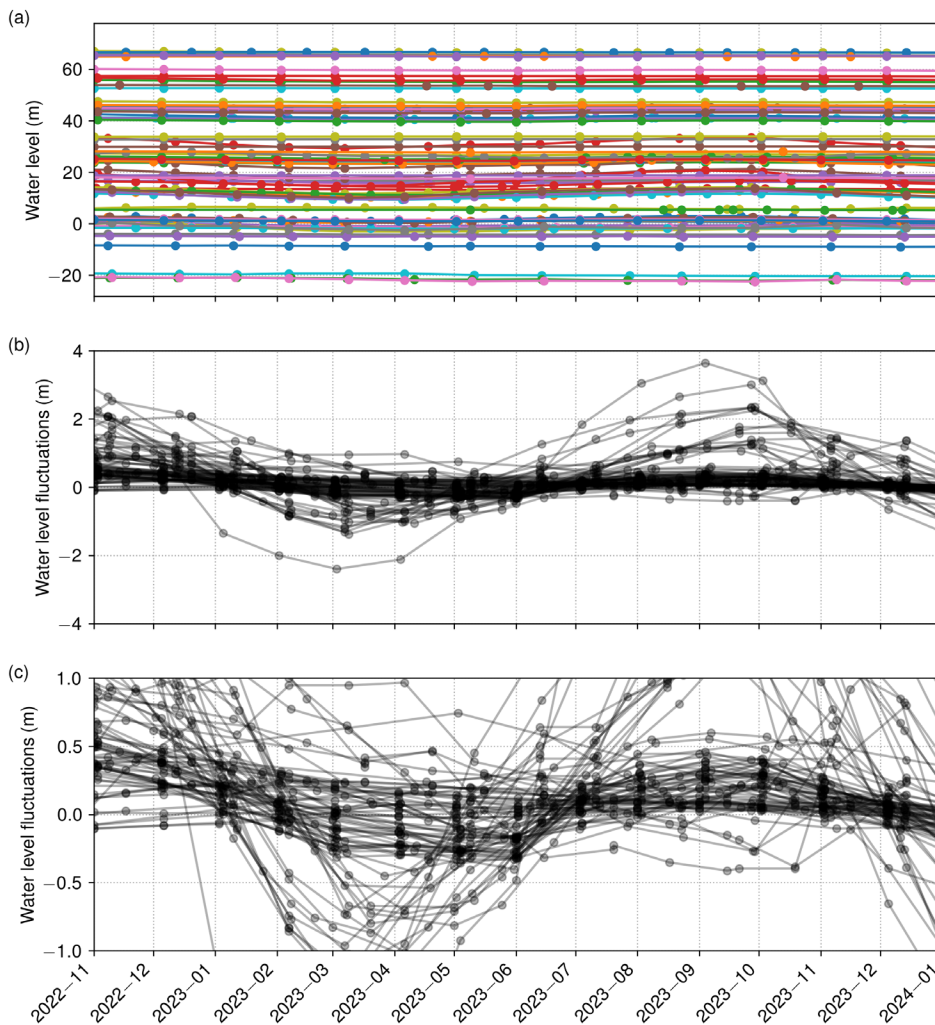


Figure 3.6. Groundwater level data measured from telemetered borehole wells near Perth. (a) shows the water level (hydraulic head) from all the 76 telemetered boreholes, with monthly data readings. Each line refers to data from one borehole. (b) shows the water level fluctuations (subtracted the average) and (c) is a zoom-in of (b).

3.3 Baseline shear-wave velocity models and depth sensitivity kernels

Yuan et al. (2025) used the ambient noise data recorded by the WA-Array to derive the shear-wave velocity model for Western Australia. Figure 3.7 shows the velocity models at different depths (0.5 km, 1 km, 1.5 and 2 km) for the Northern Perth Basin and part of the outback. The red line is the Basin boundary, which in general follow the Darling Fault. We observed a strong velocity contrast between the Perth Basin and the Yilgarn Craton in the outback, as expected that velocity in the basin is much smaller than that in the craton. The shear-wave velocity for the top 2 km depth is between 2 – 2.5 km/s for the Perth Basin, and is in general 3 – 3.8 km/s further west.

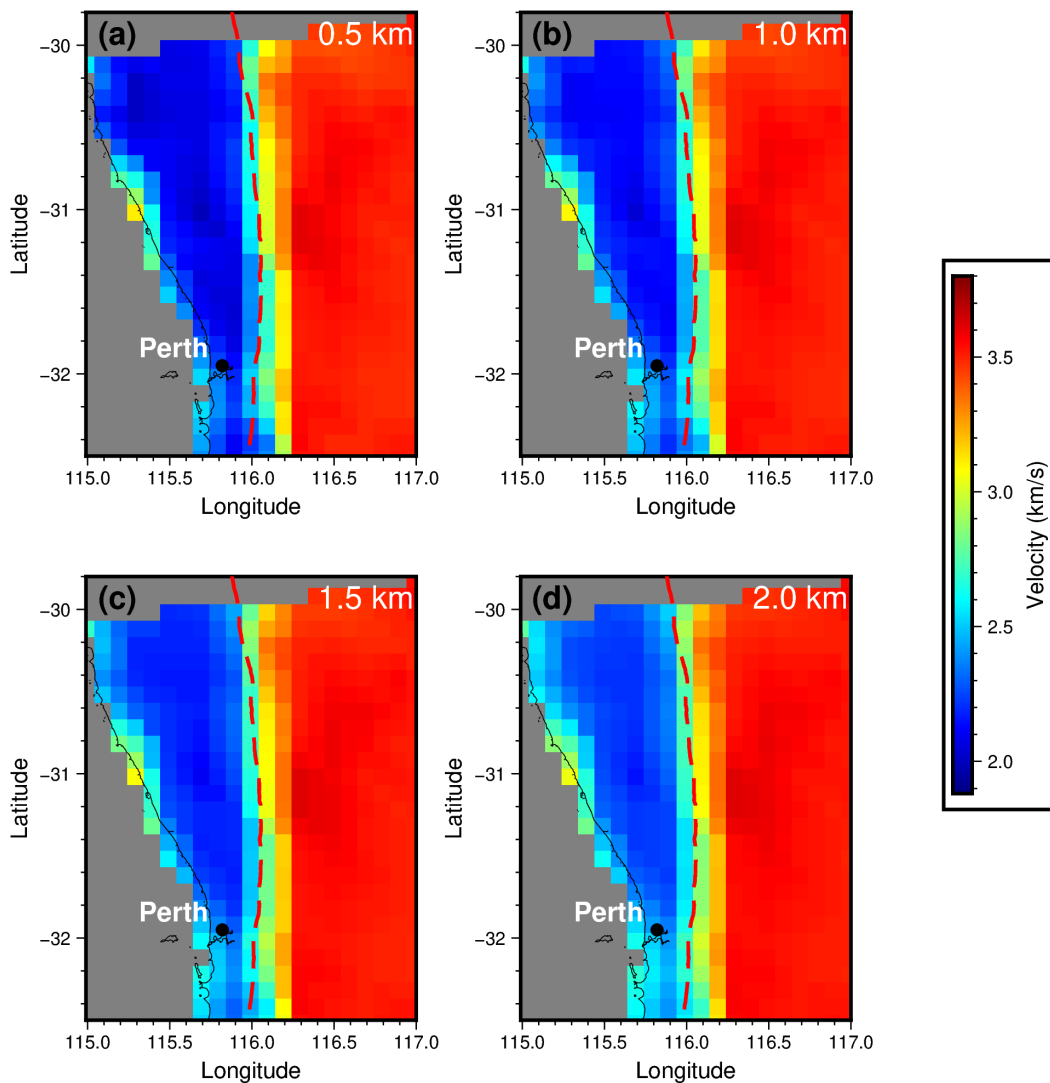


Figure 3.7. Shear-wave velocity models of the Northern Perth Basin and surrounding areas from ambient noise tomography (Yuan et al., 2025). The dashed red line indicates the boundary of the Perth Basin. The black circle refers to Perth city. (a) to (d) show velocity models corresponding to depths of 0.5 km, 1 km, 1.5 km and 2 km, respectively.

To characterise the sensitivity of Rayleigh waves for subsurface seismic velocities, we computed the depth sensitivity kernels for phase velocity using the average velocity of the Perth Basin for different frequencies (Figure 3.8). P wave velocity was estimated using an empirical relation from Brocher (2005). Using Rayleigh waves in different frequency bands, Rayleigh waves can provide information from depths. In this study, we used multiple frequency bands from 0.4 Hz to 1.6 Hz. The depth sensitivity kernels clearly show that with increasing frequency, the sensitivity of Rayleigh waves to velocities moves to shallower depths. Comparing the Rayleigh wave kernels between Perth Basin and those from the nearby Yilgarn craton, we found that for the same frequency, the sensitivity depth of Rayleigh waves is shallower depth in the Northern Perth Basin than its west (compare Figures 3.8 and 3.9).

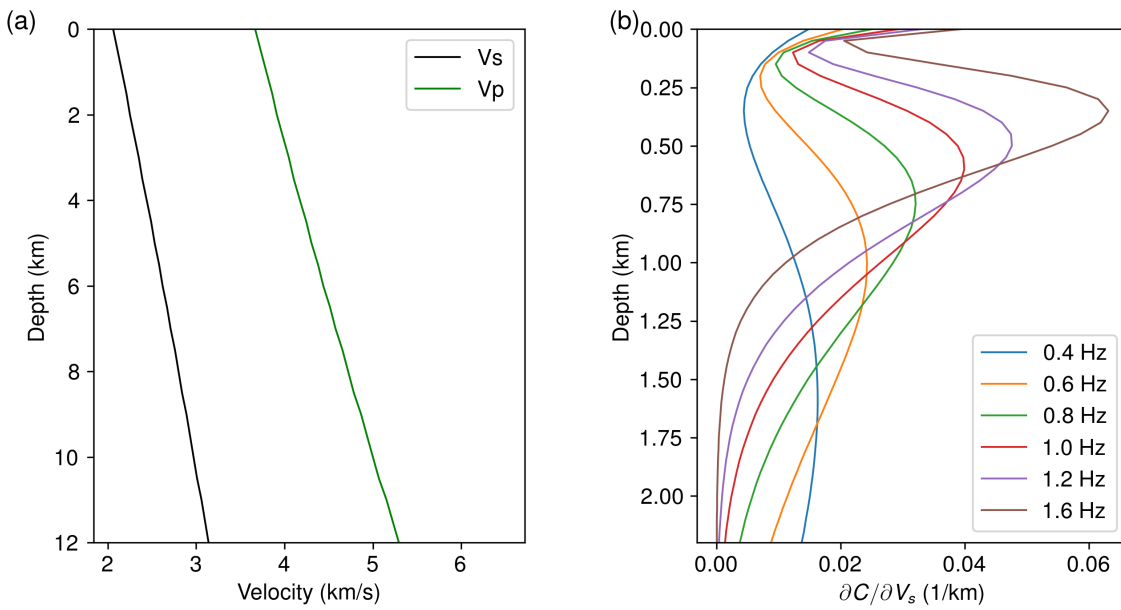


Figure 3.8. The depth sensitivity kernels of the Rayleigh waves in the Northern Perth Basin. The S-wave velocity model was from Yuan et al. (2025) and the P-wave velocity was estimated using an empirical relation in Brocher (2005).

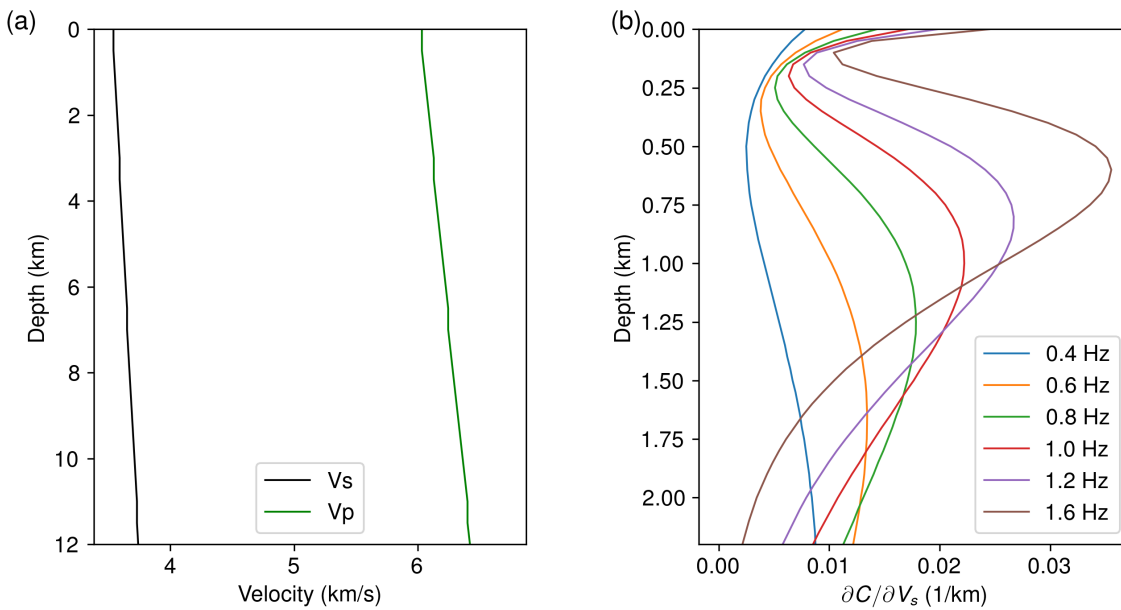


Figure 3.9. The depth sensitivity kernels of the Rayleigh waves for the Yilgarn Craton (west of 117.5 W longitude). The S-wave velocity model was from Yuan et al. (2025) and the P-wave velocity was estimated using an empirical relation in Brocher (2005).

3.4 Monitoring groundwater level changes using seismic waves

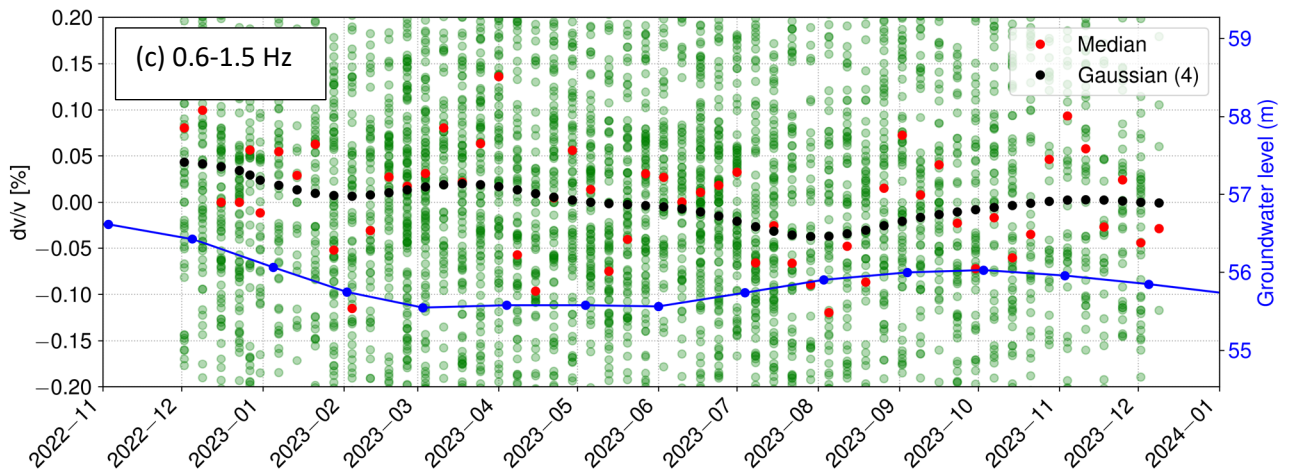
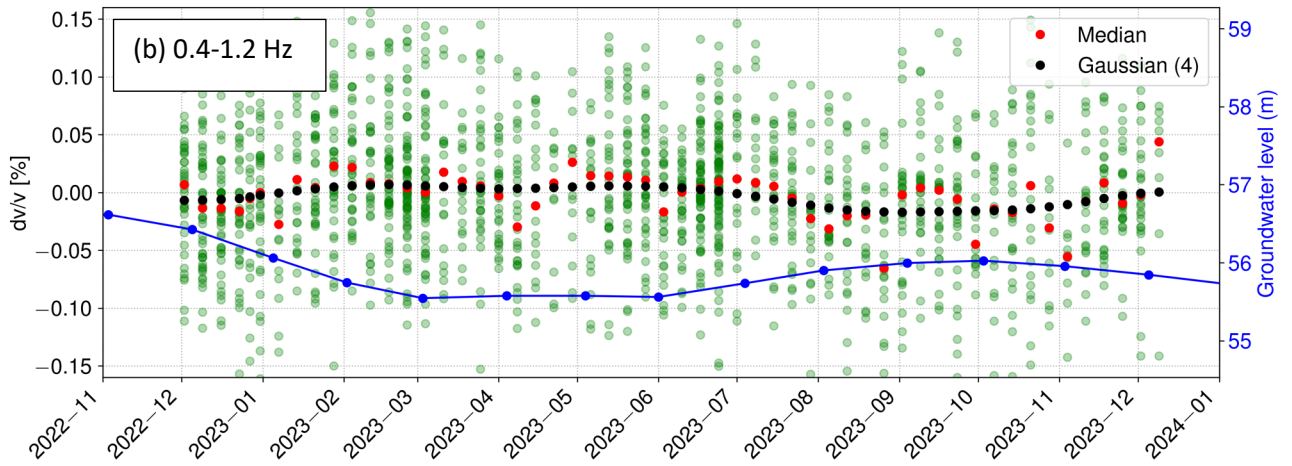
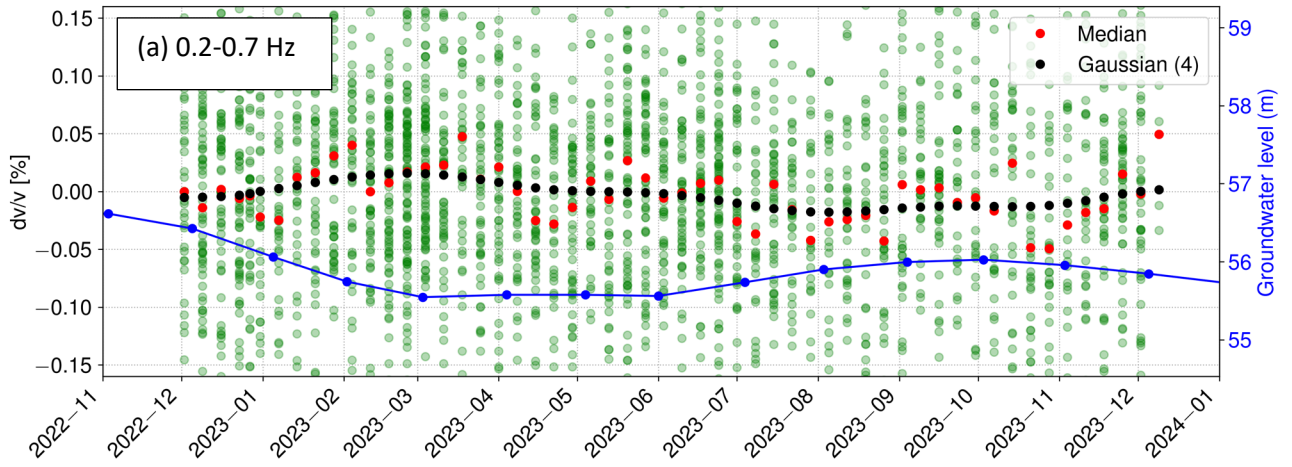
Temporal changes in subsurface properties, such as seismic wave speeds, can be monitored by measuring phase shifts in the direct arrivals and the coda (multiple scatterings) of seismic

waveforms. Continuously recorded seismic data with a duration of 1 year from WA-Array provides an unique opportunity for monitoring velocity changes in the Northern Perth Basin. The temporal seismic velocity variations provide insights for groundwater level changes. From rock-physics measurement, the shear-wave velocity decrease with increasing water saturation in the rock formations (for example, during raining season in the winter) and increase with decreasing water saturation during the dry seasons. Recently seismic method has become an emerging tool for tracking groundwater level in depth (Clements & Denolle 2018; Mao et al., 2022).

The details of the data processing steps are given in Section 3.1, which was used to obtain the monitoring data (at a fortnight interval with 7 days overlaps from December 2022 to December 2023) and baseline data. We used the early coda arrivals (15-~40 s after the first arrival) for monitoring velocity changes. The wavelet-domain trace stretching method (Yuan et al., 2021; Guo et al., 2024) was used to measure the time shift from monitoring and reference data and derive velocity changes. We used an 8-s window for comparing waveforms. In each station pair, we made 6 measurements with a 25% overlap in the time window. Like most of the literatures for subsurface passive monitoring, we did not use the direct arrivals as it is more sensitive to temporal variations from ambient seismic noise source changes, which could contaminate the measurements of velocity changes. Coda waves are the late arrivals resulted from multiply scattered waves, therefore is considered less sensitive to seismic source changes (Mao et al., 2022; Guo et al., 2024).

3.4.1 Temporal seismic velocity changes

We measured velocity changes (dv/v) for all the station pairs for different frequency bands of 0.2-0.7 Hz, 0.4 – 1.2 Hz and 0.6 - 1.5 Hz (Figure 3.10a-3.10c). We calculated velocity changes for different frequency bands, because for Rayleigh waves, different frequencies have its unique sensitivity depths for seismic velocities. Figure 3.10 shows measured velocity variations (red dots), along with groundwater level measurement (mAHD) from a borehole (blue line). We also smoothed the median velocity changes using a Gaussian filter, with the standard deviation of the Gaussian kernel to be 4. The smoothed velocity changes were reported in black in Figure 3b. We found that there was a clear pattern of shear-wave velocity decrease between July to October of 2023 (black dots and red line), which is the raining season in Perth with an overall higher groundwater level. Moreover, we found that the time-lapse seismic velocity changes become more pronounced with increasing seismic frequencies, i.e., at the shallower depth. Overall, the velocity changes are inversely correlated to groundwater levels. On the other hand, due to the station spacing, the measured velocity changes were quite noisy (probably due to the ~40 station spacing) and a Gaussian smoothing has to be applied to make sense of the results. We also compare with the dv/v measurements (Figure 3.10d) from the control group (seismic stations in the right black rectangle in Figure 3.1 further west in the outback). The dv/v is noisier in Figure 3.10d without a clear pattern. We suggest that the non-invasive, environmentally friendly and cost-effective seismic monitoring method provides a complementary solution to the traditional point-based borehole measurement. The good agreement between dv/v and the hydraulic head highlights the promising potential of using seismometer arrays in Western Australia for monitoring groundwater levels.



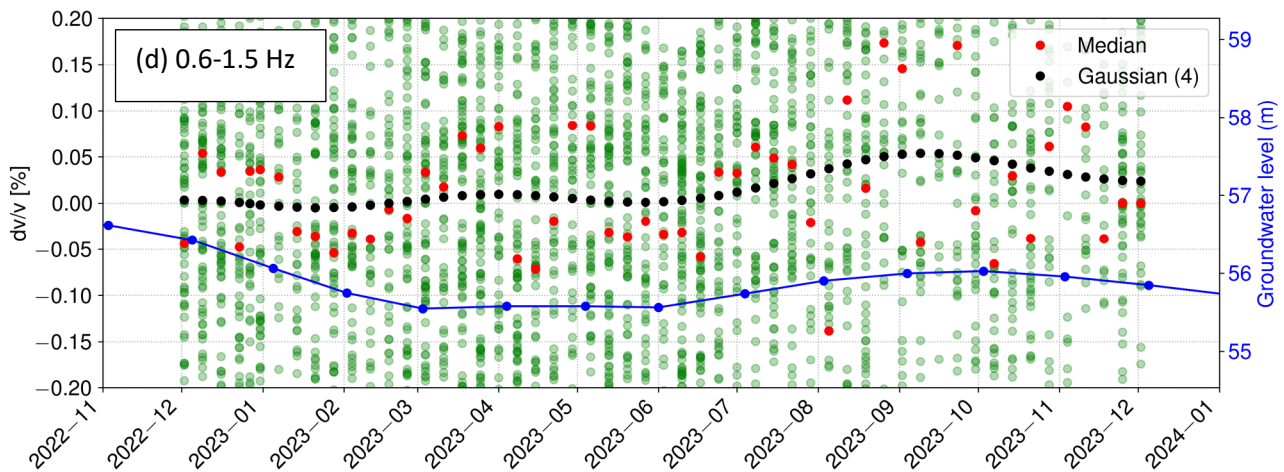


Figure 3.10. Temporal seismic velocity changes measured from time-lapse fortnight cross correlations. (a), (b) and (c) were from station pairs in the study area of interest (the left black rectangle in Figure 3.1) for 0.2-0.7 Hz, 0.4-1.2 Hz and 0.6-1.5 Hz, respectively. (d) was from further west away from the Northern Perth Basin (the right black rectangle in Figure 3.1). The overlap of each fortnight monitoring was 7 days. The blue curve was a groundwater level changes from a borehole reading in the Perth metropolitan. Each of the green dot was a measurement from a coda wave segment in a station pair. The red dots were median and the black dots were the smoothed median values using Gaussian smoothing, with the standard deviation of the Gaussian kernel to be 4.

3.4.2 Spatial distribution of velocity changes

WA-Array was designed to study the lithosphere structure of WA. With the limited number of seismometers in the Northern Perth Basin, it is challenging to provide a spatial map of groundwater levels, especially with the strong heterogeneity of groundwater level even for a small area (Figure 3.6). Using seismic waves for tracking groundwater level is an emerging technique. For most of the studies so far, the seismic station spacing is much smaller (1-5 km) than what we used here (~40 km, and we have only 9 seismic stations for the Northern Perth Basin). With the data density being so sparse, obtaining the spatial distribution of velocity changes are difficult. Here we plotted the measured velocity changes along the line connecting the station pair in Figure 3.11. In March-April, we found that the velocity changes were largely positive, while in the raining August-September, most of the velocity changes were negative. There were exceptions, probably due to the local stress heterogeneities in these regions. Some of the stations pairs, within the 100 km maximum distance, were not connected because there were no data or the data quality is not sufficiently good enough for time-lapse study.

Albeit the seismic station spacing is not ideal for spatial distribution study for the purpose of groundwater tracking, we performed a checkerboard tests (Figure 3.12). We introduced a 'true' velocity changes (Figure 3.12b) to the baseline model (Figure 3.12a). The perturbed velocity model was used for generating synthetic data, which were used as 'observed' data for a synthetic seismic inversion. We observed strong footprints (Figure 3.12c) due to the station spacing (the ~40 km station spacing was considered dense for continental study however was too large for

tracking groundwater levels in space). The estimated velocity changes are mainly along the lines connecting station pairs extended a width of one wavelength.

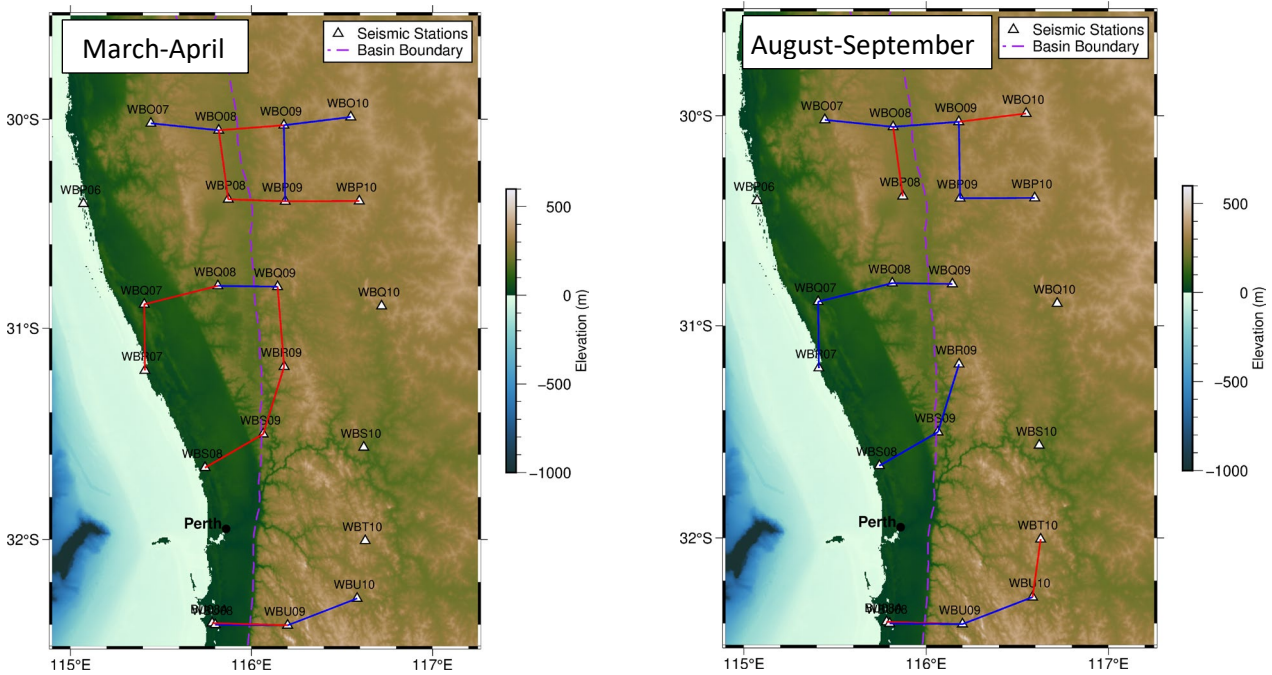


Figure 3.11. The spatial distribution of median velocity changes for frequency band 0.4 – 1.2 Hz. (a) is for data from March and April and (b) is for data from August to September. The red lines suggest positive velocity changes (velocity increases) and the blue lines suggest negative velocity changes (velocity decreases).

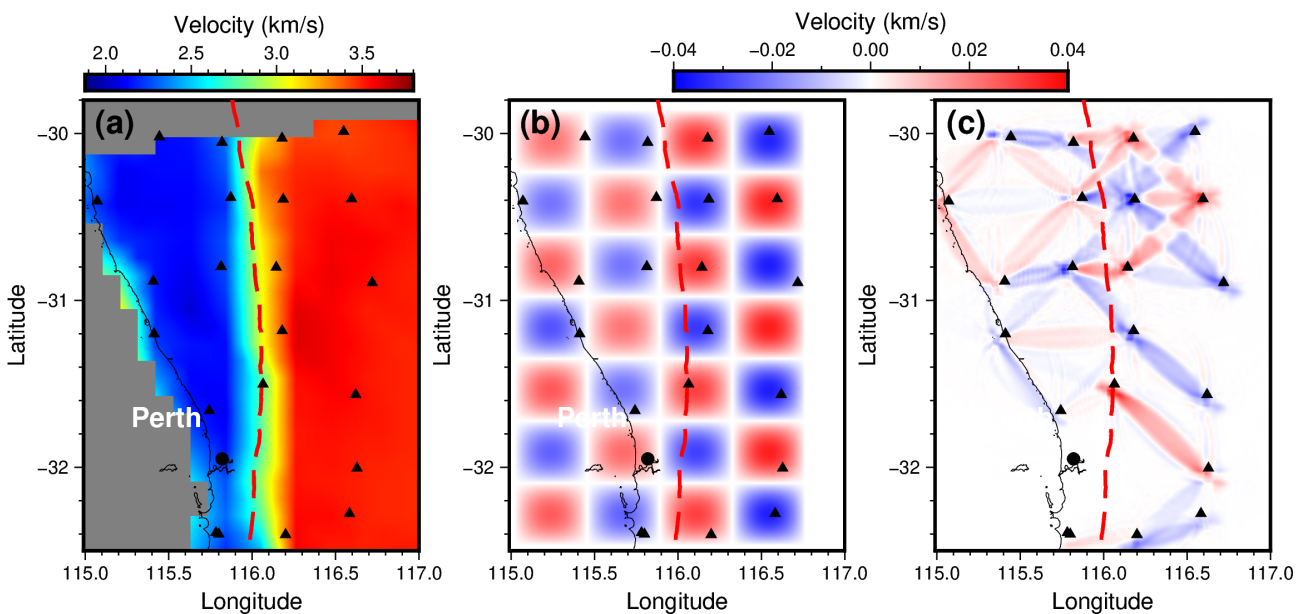


Figure 3.12. checkerboard tests for mapping the time-lapse velocity changes in space. (a) the baseline velocity, (b) the ‘true’ velocity changes, the anomaly size is 20 km by 20 km with a magnitude relative to baseline velocity of ~1%. (c) shows the estimated velocity changes using seismic inversion methods.

4 Seismicity detection, phase picking and phase association

4.1 Introduction

Seismicity refers to the patterns, frequency, and characteristics of earthquakes occurring within a specific region. It involves monitoring seismic activity and understanding the processes behind ground shaking and fault movements over time. Seismicity varies from one location to another and is influenced by factors such as tectonic plate interactions, geological structures, and human activities like resource extraction. Ground motion is typically recorded using seismometers located at seismic stations. Seismicity is commonly quantified by the magnitude and frequency of earthquakes. Regions with higher seismicity are generally more susceptible to earthquakes, making it essential to study seismicity for effective disaster preparedness and risk mitigation. Seismic data also play a vital role in informing government decisions on infrastructure development and planning. The aim of this activity is to establish a baseline catalogue of seismic activity in the region to differentiate naturally occurring earthquakes from those potentially induced by increased human activities, such as exploration and resource extraction. In the following sections, we provide a brief overview of the process for establishing an earthquake catalogue, which includes earthquake detection and phase picking, phase association, and the estimation of earthquake locations and magnitudes.

4.2 Earthquake detection and phase picking

Earthquake detection involves distinguishing true earthquake signals from the background noise and other non-earthquake sources recorded by a seismic sensor. In contrast, phase picking refers to identifying the precise arrival times of seismic phases—most notably the P-wave and S-wave—within a detected earthquake signal. These arrival times are crucial for accurately locating the earthquake source. For this study, we employed the EQTransformer model (Mousavi et al., 2020), a state-of-the-art deep learning algorithm capable of simultaneously detecting earthquake signals and picking the initial P and S phases. The model is particularly effective at identifying a greater number of smaller seismic events compared to traditional methods. EQTransformer produces output when at least one seismic phase (P or S) exceeds a user-defined probability threshold within a time window likely to contain an earthquake. We set the probability thresholds to 0.3 for detection, 0.01 for P-phase picking, and 0.01 for S-phase picking. Applying the model with these parameters to seismic data recorded by the WA-Array between November 2022 and 8 September 2024 resulted. Examples illustrating both event detection and phase picking are presented in Figures 4.1 to 4.3.

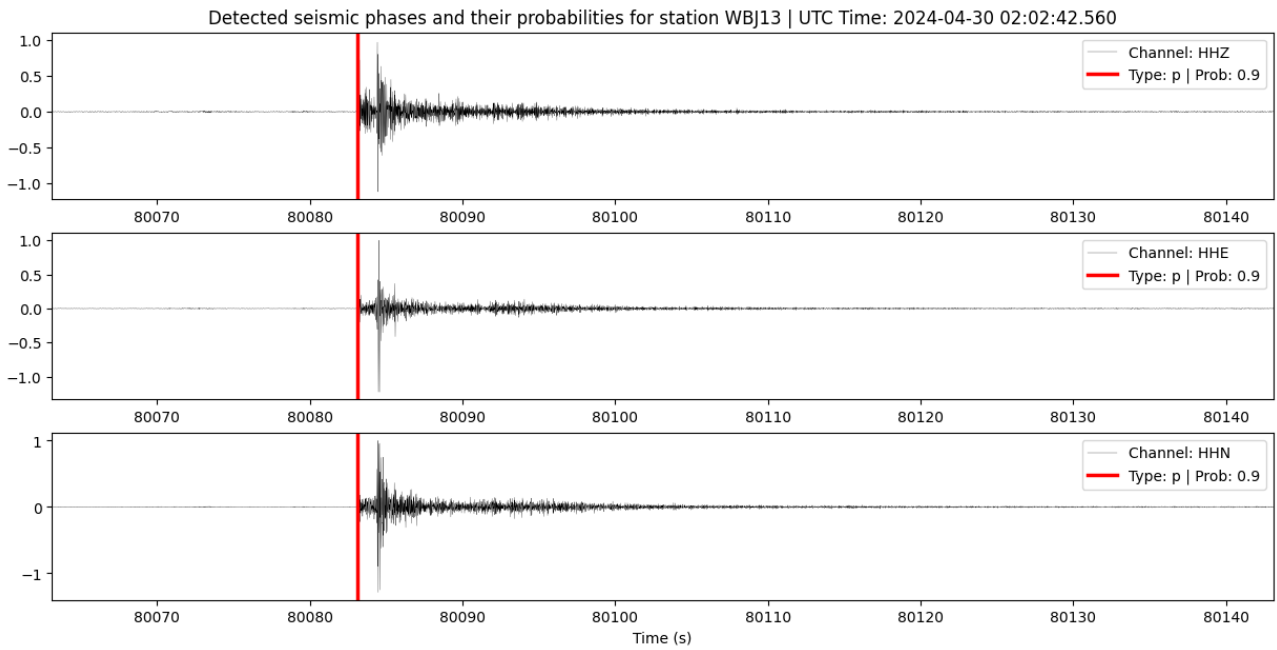


Figure 4.1. Example of a detection and P-phase pick with a 90% probability of being classified as an earthquake, recorded at station WBJ13.

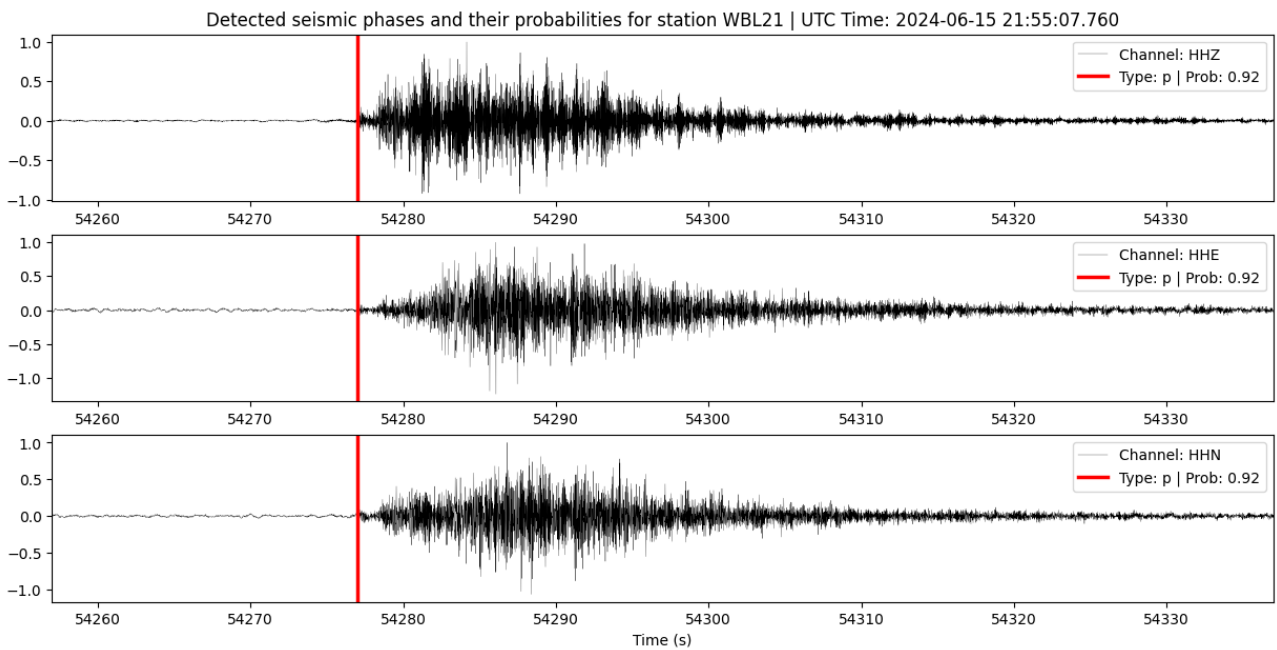


Figure 4.2. Example of a detection and P-phase pick with a 92% probability of being classified as an earthquake, recorded at station WBL21.

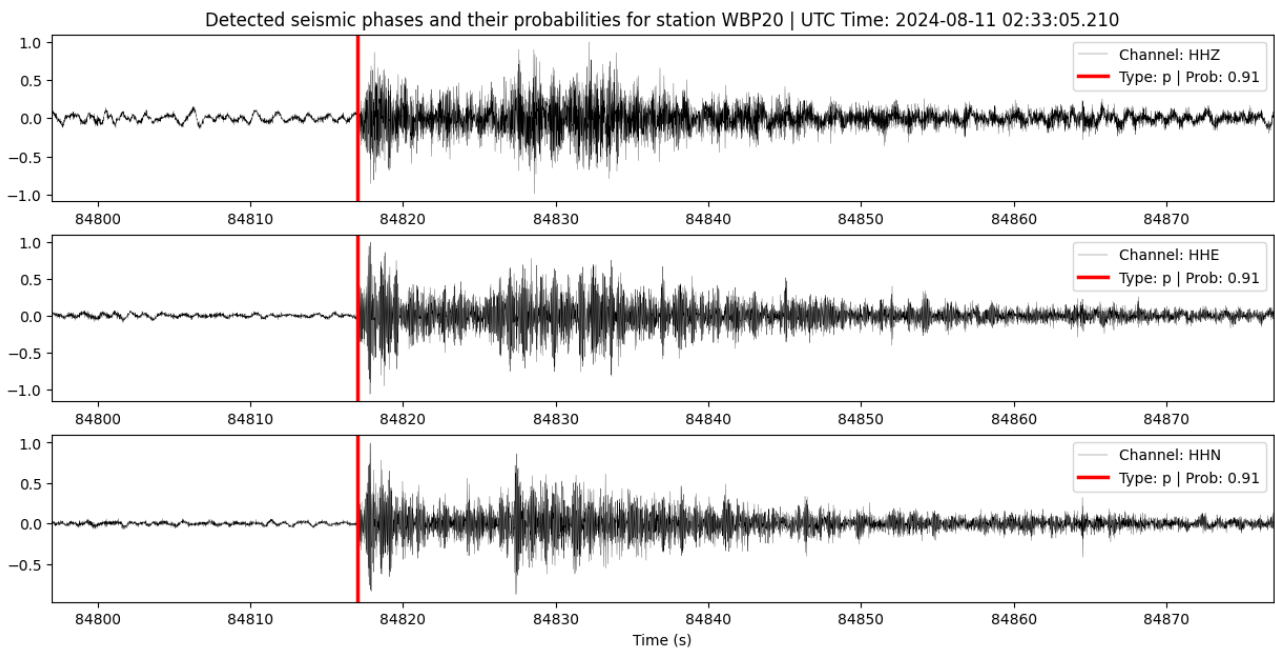


Figure 4.3. Example of a detection and P-phase pick with a 91% probability of being classified as an earthquake, recorded at station WBP20.

4.3 Phase association and initial earthquake location estimation

We filtered all detected and picked seismic phases to retain only those with a probability greater than 0.5 (50%) of being associated with an earthquake. These high-confidence picks were then used in the phase association and initial earthquake location steps.

In seismology, phase association is the process of linking seismic phases—such as P-waves and S-waves—recorded at different stations to the same seismic event. The goal is to determine which arrival times across the network correspond to a single earthquake. This is typically achieved by evaluating the consistency of arrival time differences between phases (e.g., P–S intervals) across multiple stations. Phase association also helps to identify spurious and filter through them. Accurate phase association is a critical prerequisite for earthquake location, as misassociated phases will lead to incorrect location estimates. Earthquake location estimation involves determining the epicentre, depth, and origin time of an event, using the arrival times of seismic phases recorded at different stations. Common methods include triangulation, inverse modelling, and grid search algorithms, all of which rely on seismic wave travel times computed through velocity models (e.g., homogeneous, 1D, or 3D Earth models).

For this study, we used PyOcto (Münchmeyer, 2024), a modern, Python-based phase associator inspired by the Octotree data structure. PyOcto efficiently partitions space-time into potential origin points and focuses computational effort on the most promising regions. This design allows for high-throughput phase association, mimicking grid-search methods while avoiding unnecessary computation.

To estimate preliminary earthquake locations, we employed a homogeneous velocity model with P-wave velocity (V_p) = 7 km/s and S-wave velocity (V_s) = 4 km/s, allowing a tolerance of ± 2.5 km/s. Only earthquakes occurring at depths shallower than 21 km were retained for further analysis as typical earthquake depths in this part of the continent tend to be very shallow; ~ 5 -10 km (Clarke

et al. 2014). This approach yielded 18729 seismic P and S phases recorded on all stations with high probabilities of being genuine earthquakes. Please note that this refers to the number of seismic phases recorded across many stations, not the number of distinct earthquake events. A single earthquake can generate one or more seismic P-phase or S-phase (or both) that are detected by multiple stations, so the actual number of earthquakes is likely much smaller than the total number of recorded phases.

Figure 4.4 displays the resulting initial earthquake catalogue, showing estimated locations (longitude, latitude, and depth). Several distinct earthquake clusters were observed across the region. For example:

1. Multiple clusters appear in the Southwest Seismic Zone (SWSZ), approximately 150 km east of Perth—one of Australia’s most seismically active regions.
2. A concentration of events is also found near Arthur River (red circle), between Darkan and Wagin, where earthquakes commonly occur in swarms.
3. Additionally, the region southeast of Wagin, bounded by 117°–118° longitude and 33°–34°30’S latitude (orange circle), appears to exhibit notable seismic activity.
4. Multiple clusters of seismic events related to mining activity—such as mine blasts—have been identified in areas including the Boddington Gold Mine east of the Dwellingup State Forest (black circle), Collie (east of Bunbury; blue circle), and several other locations including Kalgoorlie (green circle).

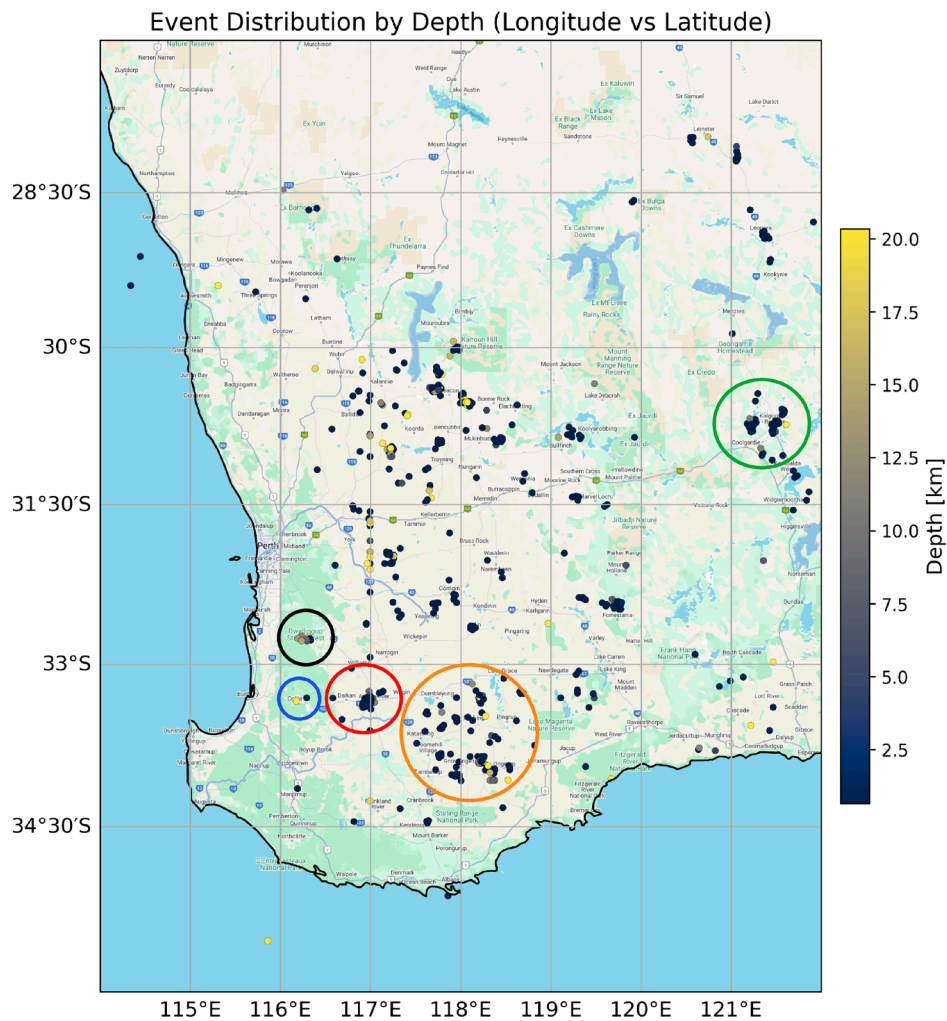


Figure 4.4. The resulting initial earthquake catalogue after phase association stage. Earthquakes within the red and orange circled areas are primarily associated with natural swarm activity, whereas the black, blue, and green circled areas indicate seismicity related to mine blasts.

5 Estimation of Earthquake Hypocentres

5.1 The absolute earthquake locations

In the previous section, we associated seismic phases identified using a deep learning algorithm with seismic events—or earthquakes—recorded across multiple stations. In this section, we focus on refining the locations of these earthquakes, specifically their hypocentres. The hypocentre is the point within the Earth where the earthquake originates and is defined by its longitude, latitude, and depth (X, Y, Z).

Determining the hypocentre is more complex than simply picking the arrival times of the P- and S-waves at various stations. Once the arrival times of the relevant seismic phases are identified, we use a seismic velocity model of the region to simulate how seismic waves propagate from an initial hypocentre. For this purpose, we use a recent shear-wave velocity (V_s) model for the Australian

continent developed by CSIRO (Chen et al., 2023), along with a compressional-wave velocity (V_p) model derived from the V_s data and the AuSREM V_p/V_s model. These models describe how fast seismic waves travel through the Earth's interior at different depths. A computer algorithm then compares the simulated arrival times at each station with the actual arrival times picked by the machine learning algorithm. The differences between them are referred to as the misfit. The algorithm iteratively adjusts the hypocentre, running new simulations and calculating updated misfits, until it finds the location that minimises the discrepancy between the observed and simulated data. This final location is considered the most accurate estimate of the earthquake's hypocentre. Depending on the earthquake's size and the number of recording stations, this process can take several hours to converge on a solution.

We use HYPOINVERSE (Fred Klein, 2002), a program developed by the US Geological Survey (USGS), to locate earthquake hypocentres. It is widely adopted by seismic networks and researchers, particularly for processing local earthquake data (e.g., Southern California Earthquake Data Centre [SCEDC], Hutton et al., 2006). However, due to uncertainties in the seismic velocity model and the picked arrival times of P- and S-waves, the estimated earthquake location will be never exact. This type of “independent” or “absolute” earthquake location is generally sufficient for routine analysis.

In certain cases, however—especially when seismicity is tightly clustered in space and time, such as during earthquake swarms or aftershock sequences—we can significantly improve location accuracy by simultaneously locating a group of nearby earthquakes relative to each other. This method is known as relative location or relocation, which we implement in the next step.

5.2 The relative location of earthquakes or precise location?

Relative relocation helps mitigate the influence of unmodelled complexities in the seismic velocity structure (e.g., 3D velocity variations). By focusing on the small differences in arrival times between earthquakes recorded across the same network, we can more precisely attribute these differences to actual variations in earthquake locations. When many earthquakes are relocated simultaneously, we can construct an optimal network of relative positions. This improves the stability of the solutions and reduces the impact of errors in picking P- and S-wave onsets.

High-precision earthquake locations can yield important scientific insights. For instance, they can reveal systematic migration patterns within earthquake swarms or indicate whether earthquakes are occurring along a single fault, a complex fault system, or throughout a broader volume of crust. These spatial patterns help researchers infer the underlying physical processes driving the seismicity—such as stress transfer, elevated pore-fluid pressure, or magma intrusion. This in turn provides valuable information about dynamic subsurface processes, which is critical for understanding both seismic and volcanic hazards.

We use HypoDD, a Fortran-based software package for earthquake relocation using the double-difference (DD) algorithm (Waldhauser and Ellsworth, 2000). This method leverages the principle that if the separation between two earthquake hypocentres is small relative to the event-station distance and the scale of velocity heterogeneity in the Earth, then the seismic waves from both events will travel along nearly identical ray paths to a given station. As a result, the difference in travel times between the two events at a common station—known as the double-difference—is primarily due to differences in their relative locations and origin times. By minimising these

double-difference residuals across a network of stations, the algorithm refines the relative positions of earthquake pairs with high precision.

Figure 5.1 presents the final earthquake catalogue generated using the HypoDD package. Only seismic events with a high probability of being genuine earthquakes were included. In the final project report, the initial catalogue will be refined following phase association. As a result, the final catalogue may differ slightly; while we do not expect significant changes in the locations of the current events, the total number of earthquakes may increase if additional events are identified in the revised initial catalogue.

Figure 5.2 shows a closer view of seismicity within the study area in the Northern Perth Basin (outlined by the black rectangle). As shown, there are no significant concentrations of earthquakes within the Northern Perth Basin itself. However, just east of the area, the seismicity map reveals several small clusters of earthquakes. The cluster near the town of Three Springs is associated with Talc Mine site exploration activities, while the others are likely related to natural earthquake swarm activity in the region. Examples of these natural seismicity clusters include those located between Latham and Perenjori, in and around eastern Dalwallinu, and near Rothsay.

Distribution of seismicity (with probability > 50%) by Depth and Magnitude

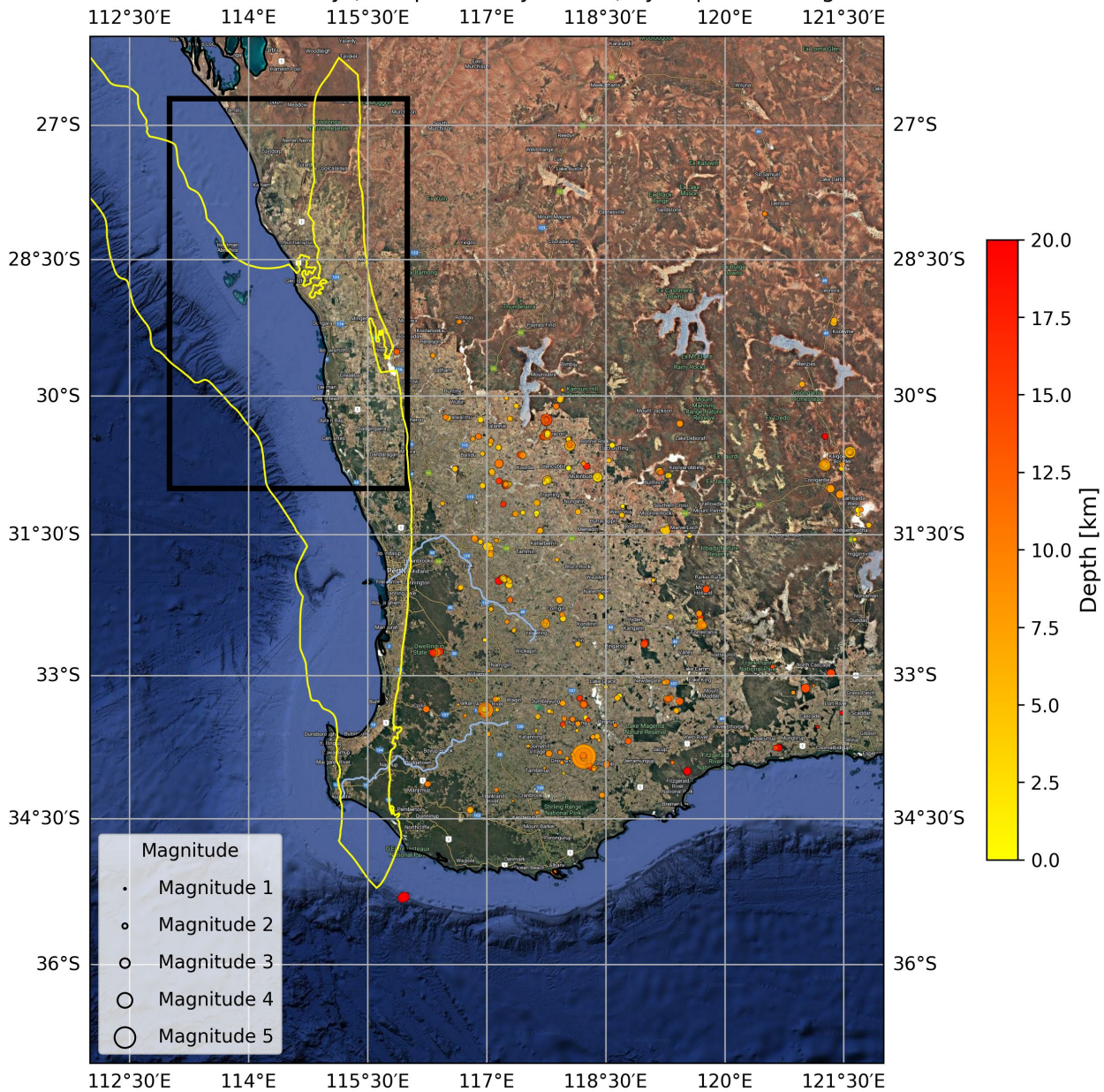


Figure 5.1. The final earthquake catalogue showing high-probability seismic events in the region. The yellow line outlines the extent of the Perth Basin, while the black rectangle highlights the study area located within the Northern Perth Basin.

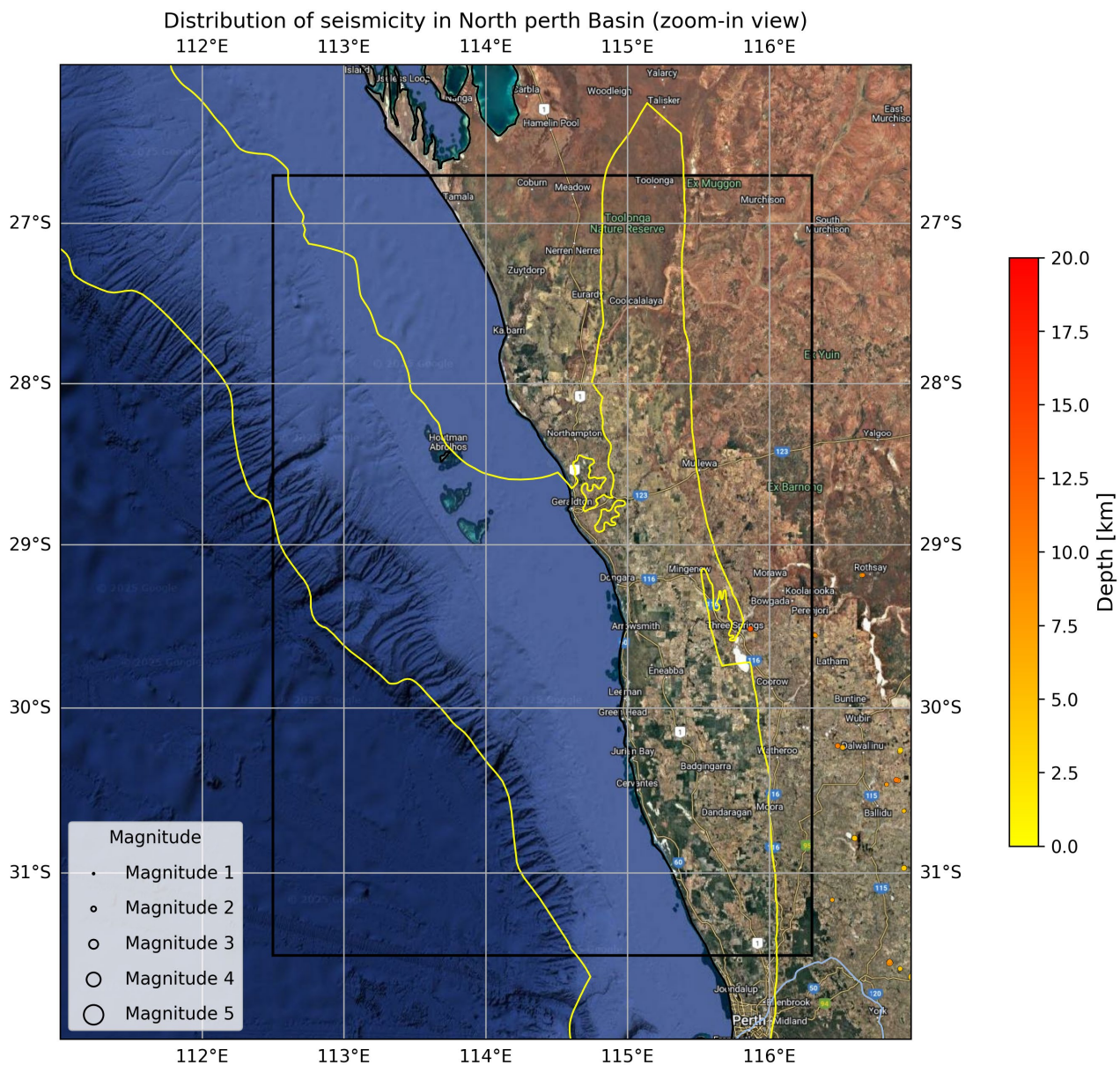


Figure 5.2. Map showing clusters of natural seismicity within and around the study area in the Northern Perth Basin. Notable clusters are observed between Latham and Perenjori, in the vicinity of eastern Dalwallinu, and near Rothsay. No significant seismic activity is recorded within the Northern Perth Basin itself, which is outlined by the yellow boundary.

References:

- Bensen, G. D., Ritzwoller, M. H., Barmin, M. P., Levshin, A. L., Lin, F., Moschetti, M. P., ... & Yang, Y. (2007). Processing seismic ambient noise data to obtain reliable broad-band surface wave dispersion measurements. *Geophysical journal international*, 169(3), 1239-1260.
- Brocher, T. M. (2005). Empirical relations between elastic wavespeeds and density in the Earth's crust. *Bulletin of the seismological Society of America*, 95(6), 2081-2092.
- Clark, D., McPherson, A., Allen, T., & Talwani, P. (2014). Intraplate earthquakes in Australia. *Intraplate earthquakes*, 8-49.
- Clements, T., & Denolle, M. A. (2018). Tracking groundwater levels using the ambient seismic field. *Geophysical Research Letters*, 45(13), 6459-6465.

Delevingne, L., Glazener, W., Grégoir, L., & Henderson, K. (2020). Climate risk and decarbonization: What every mining CEO needs to know. McKinsey Insights.

Department of Water, 2017, Northern Perth Basin: Geology, hydrogeology and groundwater resources, Hydrogeological bulletin series, report no. HB1, Department of Water, Government of Western Australia, Perth.

Doussan, C., Vercambre, G., & Pagès, L. (1999). Water uptake by two contrasting root systems (maize, peach tree): results from a model of hydraulic architecture. *Agronomie*, 19(3-4), 255-263.

Guo, P., Saygin, E., & Kennett, B. (2024). Space-time monitoring of seafloor velocity changes using seismic ambient noise. *Journal of Geophysical Research: Solid Earth*, 129(6), e2023JB027953.

Guo, Peng; Tork Qashqai, Mehdi; Saygin, Erdinc. Establishing Baseline Groundwater and Natural Seismicity levels across the Northern Perth Basin with Passive Seismic Data – Interim Report 1 .

<https://gisera.csiro.au/research/surface-and-groundwater/baseline-groundwater-and-seismicity-of-northern-perth-basin/>: CSIRO; 2024. csiro:EP2024-5150.

<http://hdl.handle.net/102.100.100/660339?index=1>

Knight, R., and A. L. Endres (2005), An introduction to rock physics for near-surface applications, in *Near-Surface Geophysics*, vol. 1, Concepts and Fundamentals, edited by D. Butler, pp. 31–70, Soc. of Explor. Geophys., Tulsa, Okla

Miller, M. S., Pickle, R., Murdie, R., Yuan, H., Allen, T. I., Gessner, K. & Whitney, J. (2023). Southwest Australia Seismic Network (SWAN): Recording earthquakes in Australia’s most active seismic zone. *Seismological Society of America*, 94(2A), 999-1011.

Mousavi, S.M., Ellsworth, W.L., Zhu, W. *et al.* Earthquake transformer—an attentive deep-learning model for simultaneous earthquake detection and phase picking. *Nat Commun* 11, 3952 (2020).

<https://doi.org/10.1038/s41467-020-17591-w>.

Mao, S., Lecointre, A., van der Hilst, R. D., & Campillo, M. (2022). Space-time monitoring of groundwater fluctuations with passive seismic interferometry. *Nature communications*, 13(1), 4643.

Münchmeyer, J. (2024). PyOcto: A high-throughput seismic phase associator. *Seismica*,

<https://doi.org/10.26443/seismica.v3i1.1130> .

Park, C. B., Miller, R. D., Xia, J., & Ivanov, J. (2007). Multichannel analysis of surface waves (MASW)—active and passive methods. *The leading edge*, 26(1), 60-64.

Parker, A. L., Filmer, M. S., & Featherstone, W. E. (2017). First results from Sentinel-1A InSAR over Australia: application to the Perth Basin. *Remote Sensing*, 9(3), 299.

Yuan, C., Bryan, J., & Denolle, M. (2021). Numerical comparison of time-, frequency- and wavelet-domain methods for coda wave interferometry. *Geophysical Journal International*, 226(2), 828-846.

Yuan, H., R.E. Murdie, M.S. Miller, T. Li and K. Gessner (2025). Chapter 11. Crustal shear-wave velocity model. WA Array Phase 1 – Southwest.

As Australia's national science agency and innovation catalyst, CSIRO is solving the greatest challenges through innovative science and technology.

CSIRO. Unlocking a better future for everyone.

Contact us

1300 363 400
+61 3 9545 2176
csiro.au

For further information

1300 363 400
gisera.csiro.au

GISERA is a collaboration between CSIRO, Commonwealth and state governments and industry established to undertake publicly-reported independent research. The purpose of GISERA is to provide quality assured scientific research and information to communities living in gas development regions focusing on social and environmental topics including: groundwater and surface water, greenhouse gas emissions, biodiversity, land management, the marine environment, and socio-economic impacts. The governance structure for GISERA is designed to provide for and protect research independence and transparency of research.